2018 22nd International Conference on System Theory, Control and Computing (ICSTCC)

Project and Design of Multi-Rate Loop Controllers for Fixed-Wings Aircrafts

M. F. Santos*, D. H. C. Silva†, M. F. Silva‡, V. F. Vidal§, L. M. Honório¶,
V. L. M. Lopes ∥ L. A. Z. Silva **, H. B. Rezende††, J. M. S. Ribeiro ‡‡, A. S. Cerqueira[x],
A. A. N. Pancoti[xi], B. A. Regina[xii]

Centro Federal de Educação Tecnológica de Minas Gerais,
CEFET-MG, Leopoldina, MG, 36700-000, Brazil
murillo@leopoldina.cefetmg.br*, danielcalado94@gmail.com†

Juiz de Fora Federal University,
UFJF, Juiz de Fora, MG, 36036-900, Brazil
mathausfsilva@hotmail.com‡, vinicius.vidal@engenharia.ufjf.br§, leonardo.honorio@ufjf.edu.br¶,
vmainenti@gmail.com∥, luiz.zillmann@engenharia.ufjf.br**, henrique.rezende@engenharia.ufjf.br††,
joao.ribeiro@engenharia.ufjf.br‡‡, augusto.santiago@ufjf.edu.br[x], antonio.pancoti@engenharia.ufjf.br[xi],
almeida.bruno@engenharia.ufjf.br[xii]

***Abstract*—This work aims to show kinematics and dynamics modelling of a fixed-wing UAV type, as well as Proportional and Proportional, Integral and Derivative controllers for multi-rate cascade control loop, one internal for angular attitude and another external for the inertial position. The control loops are designed for roll, pitch, yaw, altitude and linear velocity in forwarding and backward aircraft nose direction. These dynamics are controlled by the integration of loops in different levels using the Successive Loop Closure technique. The results were satisfactory, considering that the simulation tests took into account the parameters of an already developed aircraft.**

***Keywords*—UAV, Fixed-wings Aircraft, P/PID Controllers, Successive Loop Closure.**

I. INTRODUCTION

Unmanned Aerial Vehicles (UAVs) are aircrafts that work without the presence of a human being on-board. They can have a deliberative capacity, in varying degrees according to their sophistication and purpose of the application, to autonomously fulfil pre-programmed missions [1].

It is known, however, that the design and construction of a UAV encompass different stages, such as modelling, control, tuning of controllers, execution and validation of tests. As regards the control stage and its tuning, some recent works referring to fixed-wing UAVs deserve attention: work [2] deals with the design of five controllers, based on Backstepping and Sliding Modes, taking simulations in a fixed-wing UAV into consideration. Work [3] presents a control design for the lateral-directional dynamics of a fixed-wing aircraft, to command the lateral-directional movements to the equilibrium point that corresponds to a specific coordinated turn. Numerical simulation results were presented to show the closed-loop system behaviour. A more extensive work is presented in [4], where an approach for obtaining dynamically possible reference trajectories and feedback controllers for a fixed-wing aircraft was developed. They showed modelling, control techniques, simulation and validation through experimental results.

In these works commented previously, it was not widespread analysed and studied the influence of control loop frequencies separately, considering the cascade implementation in some cases. It is in this context that this work was developed. The main purpose here is to present the kinematics and dynamics modelling of a fixed-wing UAV, as well as Proportional (P) / Proportional, Integral and Derivative (PID) controllers for multi-rate control loops, one for angular attitude and another for the inertial position, in cascade for each dynamics. Three angular attitudes (roll, pitch and yaw) dynamics, altitude and forward/backward linear velocity are controlled. For this, the primary purpose is hereafter presented, where it is necessary to integrate loops of different frequencies, considering the slower one as a unit gain for the faster ones. In this way, the Successive Loop Closure technique is used.

II. AIRCRAFT KINEMATICS AND DYNAMICS MODELING

Typically, UAV modelling uses the following state variables: the vector $[p_n, p_e, h]^T$ represents the inertial North, East and Altitude (facing down) positions along the $(\hat{i}^i, \hat{j}^i, -\hat{k}^i)$ axes representing the inertial frame; the vector $[\phi, \theta, \psi]^T$ represents the roll, pitch and yaw angles considering the vehicle frame $(\hat{i}^v, \hat{j}^v, -\hat{k}^v)$. The vectors $[u, v, \omega]^T$ and $[p, q, r]^T$ represent the three dimensional speeds and angular velocities over the axes $(\hat{i}^b, \hat{j}^b, -\hat{k}^b)$ of the body frame [5].

A. Aircraft Kinematics Modeling

The UAV translational velocity is commonly expressed along the body-fixed frame. The components u, v and ω

correspond to the inertial velocities in the axes $\boldsymbol{i^b}$, $\boldsymbol{j^b}$ and $\boldsymbol{k^b}$, respectively. However, the UAV translational positions are usually measured and expressed in the inertial *frame* [6]. In this way, the relation between these positions and their velocities can be expressed as follows:

$$\begin{pmatrix} \dot{p}_n \\ \dot{p}_e \\ -\dot{h} \end{pmatrix} = \begin{pmatrix} c\theta c\psi & s\phi s\theta c\psi - c\theta s\psi & c\phi s\theta c\psi + s\phi s\psi \\ c\theta s\psi & s\phi s\theta s\psi + c\phi c\psi & c\phi s\theta s\psi - s\phi c\psi \\ -s\theta & s\phi s\theta & c\phi c\theta \end{pmatrix} \begin{pmatrix} u \\ v \\ \omega \end{pmatrix} \tag{1}$$

where $c\theta \triangleq \cos\theta$ and $s\theta \triangleq \sin\theta$.

The equations between angular positions (ϕ, θ and ψ) and angular velocities (p, q and r) are expressed in different frames through rotation matrices [6], [7], as shown in (2):

$$\begin{pmatrix} \dot{\phi} \\ \dot{\theta} \\ \dot{\psi} \end{pmatrix} = \begin{pmatrix} 1 & s\phi t\theta & c\phi t\theta \\ 0 & c\phi & -s\phi \\ 0 & \dfrac{s\phi}{c\theta} & \dfrac{c\phi}{c\theta} \end{pmatrix} \begin{pmatrix} p \\ q \\ r \end{pmatrix} \tag{2}$$

where $t\theta \triangleq \tan\theta$.

B. Aircraft Dynamics Modeling

Using Newton's second law, the translational and rotational movements are described in (3) (velocities in their respective axes) and in (4) (roll, pitch and yaw rates).

$$\begin{pmatrix} \dot{u} \\ \dot{v} \\ \dot{\omega} \end{pmatrix} = \begin{pmatrix} rv - q\omega \\ p\omega - ru \\ qu - pv \end{pmatrix} + \frac{1}{m_T} \begin{pmatrix} f_x \\ f_y \\ f_z \end{pmatrix} \tag{3}$$

where m_T is the UAV total mass, f_x, f_y and f_z are the resultant forces in $\boldsymbol{i^b}$, $\boldsymbol{j^b}$ and $\boldsymbol{k^b}$ axes, respectively.

$$\begin{pmatrix} \dot{p} \\ \dot{q} \\ \dot{r} \end{pmatrix} = \begin{pmatrix} \Gamma_1 pq - \Gamma_2 qr + \Gamma_3 L^b + \Gamma_4 N^b \\ \Gamma_5 pr - \Gamma_6 (p^2 - r^2) + \frac{1}{J_y} M^b \\ \Gamma_7 pq - \Gamma_1 qr + \Gamma_4 L^b + \Gamma_8 N^b \end{pmatrix} \tag{4}$$

where L^b, M^b and N^b are rolling, pitching and yawing resultant torques in the vehicle frame, consecutively; Γ_* are moments and product inertia equations, approaching to some aircraft symmetries, such as in $\boldsymbol{i^b}-\boldsymbol{k^b}$ planes ($J_{xy} = J_{yz} = 0$). J_{xy} and J_{yz} are UAV inertia products. More details about Γ_* equations are expressed in Appendix A.

According to [8], the forces and torques acting on the UAV are preliminarly caused by 3 sources: gravitational, aerodynamic and propulsion.

C. Aircraft Resultant Forces

The resultant forces acting on the vehicle body-fixed frame are the sum of gravitational, aerodynamic and propulsion forces: $\boldsymbol{f^b} = \boldsymbol{f^b_g} + \boldsymbol{f^b_p} + \boldsymbol{f^b_a}$, $\boldsymbol{f^b_g}$, where $\boldsymbol{f^b_a}$ and $\boldsymbol{f^b_p} \in \mathbb{R}^3$. According to [6], the gravitational force in the body-fixed frame is:

$$\boldsymbol{f^b_g} = \begin{pmatrix} -m_T g s\theta, m_T g c\theta s\phi, m_T g c\theta c\phi \end{pmatrix}^T \tag{5}$$

where g is the gravitational constant, considered equal to $9.81 m/sec^2$.

The propulsion forces are aligned to $\boldsymbol{i^b}$, since the propeller is placed at the UAV "nose". Using dynamics concepts, (6) represents them:

$$\boldsymbol{f^b_p} = \begin{pmatrix} \rho n^2 D^4 C_{F_T}(J), 0, 0 \end{pmatrix}^T \tag{6}$$

where ρ is the ar density, D the propeller diameter, n the engine speed, $C_{F_T}(J)$ is the dimensionless thrust coefficient, given by (7) and $J = \frac{V_T}{D\pi n}$ [8]. $V_T = \sqrt{u_T^2 + v_T^2 + w_T^2}$ is the airspeed euclidean norm, where u_T^2, v_T^2 and w_T^2 are the aircraft speeds in wind frame directions.

$$C_{F_T}(J) = C_{F_{T1}} + C_{F_{T2}} J + C_{F_{T3}} J^2 \tag{7}$$

where $C_{F_{T1}}$, $C_{F_{T2}}$ and $C_{F_{T3}}$ are shown in Table I.

The engine speed dynamics can be expressed by a first-order linear system, considering the engine speed reference signal n_c and its time constant τ_n.

$$\dot{n} = -\frac{1}{\tau_n} n + \frac{1}{\tau_n} n_c \tag{8}$$

The aerodynamic forces $\boldsymbol{f^b_a}$ are obtained through dimensionless coefficients, dynamic pressure $\bar{q}$ and wing surface area S.

$$\boldsymbol{f^b_a} = \begin{pmatrix} \bar{q} S C_X, \bar{q} S C_Y, \bar{q} S C_Z \end{pmatrix}^T \tag{9}$$

with dynamic pressure expressed by $\bar{q} = \frac{\rho V_T^2}{2}$ with:

$$\begin{aligned} C_X &= C_{X_V} + C_{X_\alpha}\alpha + C_{X_{\delta_e}}\delta_e \\ C_Y &= C_{Y_\beta}\beta + C_{Y_{\delta_r}}\delta_r + C_{Y_{\delta_a}}\delta_a + C_{Y_p}\frac{pb}{2V_T} + C_{Y_r}\frac{rb}{2V_T} \\ C_Z &= C_{Z_V} + C_{Z_\alpha}\alpha + C_{Z_{\delta_e}}\delta_e + C_{Z_{\dot{\alpha}}}\frac{\dot{\alpha}\bar{c}}{2V_T} + C_{Z_q}\frac{q\bar{c}}{2V_T} \end{aligned}$$

where b is the wingspan, $\bar{c}$ is the mean aerodynamic chord, α is the attack angle, $\dot{\alpha}$ is the attack velocity, β is the sideslip angle, and δ_a, δ_e and δ_r are control surfaces: aileron, elevator and rudder, respectively.

D. Aircraft Resultant Torques

The aircraft attitude angles are changed by torques applied to the vehicle frame through the control surfaces (δ_a, δ_e and δ_r).

$$\begin{pmatrix} L^b, M^b, N^b \end{pmatrix}^T = \begin{pmatrix} \bar{q} S b C_L, \bar{q} S \bar{c} C_M, \bar{q} S b C_N \end{pmatrix}^T \tag{10}$$

$$\begin{aligned} C_L &= C_{L_\beta}\beta + C_{L_{\delta_a}}\delta_a + C_{L_{\delta_r}}\delta_r + C_{L_p}\frac{pb}{2V_T} + C_{L_r}\frac{rb}{2V_T} \\ C_M &= C_{M_V} + C_{M_\alpha}\alpha + C_{M_{\delta_e}}\delta_e + C_{M_{\dot{\alpha}}}\frac{\dot{\alpha}\bar{c}}{2V_T} + C_{M_q}\frac{q\bar{c}}{2V_T} \\ C_N &= C_{N_\beta}\beta + C_{N_{\delta_a}}\delta_a + C_{N_{\delta_r}}\delta_r + C_{N_p}\frac{pb}{2V_T} + C_{N_r}\frac{rb}{2V_T} \end{aligned}$$

III. AIRCRAFT PROJECTED

Two preliminary parallel steps are necessary to conclude the final project, one for fixed-wing topology and another for the quadcopter. Considering the fixed-wing topology, Fig. 1 shows 2 views of the vehicle built in this work, with its constructive parameters presented in Table I.

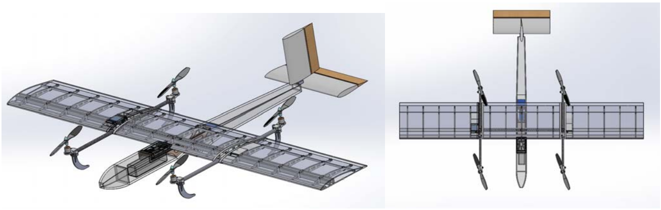

(a) Aircraft isometric view from SolidWorks software.
(b) Aircraft top view from SolidWorks software.

Figure 1. Illustrative pictures of the developed UAV.

TABLE I
AIRCRAFT CONSTRUCTIVE PARAMETERS.

Parameter	Value	Parameter	Value
m_T	$1.925Kg$	S	$0.345m^2$
$\bar{c}$	$0.23m$	b	$1.5m$
J_x	$0.10135739Kg.m^2$	J_{xy}	$0.00032572Kg.m^2$
J_y	$0.16034454Kg.m^2$	J_{xz}	$0.00004136Kg.m^2$
J_z	$0.12346079Kg.m^2$	J_{yz}	$0.00014976Kg.m^2$
C_{FT1}	8.42×10^{-2}	C_{FT1}	-1.36×10^{-1}
C_{FT3}	9.28×10^{-1}	D	$0.2m$
τ_n	$0.4sec$	t_{s1}	$0.01sec$

where t_{s1} is the fast loop step time, J_x, J_y and J_z, are the inertia moments, J_{xy}, J_{xz} and J_{yz} are the inertia products.

Regarding the aerodynamic concepts, the aircraft stability derivatives are obtained through a specific simulation software, used before wind tunnel tests. Their coefficients are shown in Table II.

TABLE II
AIRCRAFT DIMENSIONLESS AERODYNAMICS COEFFICIENTS.

Parameter	Value	Parameter	Value
C_{X_V}	-0.016323	C_{X_α}	0.22213
$C_{X_{\delta_e}}$	0	C_{Y_β}	-0.15173
C_{Y_p}	0.030158	C_{Y_r}	0.13172
$C_{Y_{\delta_r}}$	0	$C_{Y_{\delta_a}}$	0
C_{Z_V}	-0.00023305	C_{Z_α}	4.659
C_{Z_q}	6.9671	$C_{Z_{\delta_e}}$	0
$C_{Z_{\dot{\alpha}}}$	6.9671	C_{L_β}	-0.0041764
$C_{L_{\delta_a}}$	0	$C_{L_{\delta_r}}$	0
C_{L_p}	-0.47063	C_{L_r}	0.10709
C_{M_V}	0	C_{M_α}	-0.74061
$C_{M_{\dot{\alpha}}}$	-0.82081	C_{M_q}	-8.2081
$C_{M_{\delta_e}}$	0	C_{N_β}	0.05969
$C_{N_{\delta_a}}$	0	$C_{N_{\delta_r}}$	0
C_{N_β}	0.05969	C_{N_p}	-0.068942
C_{N_r}	-0.052307		

More details about UAV modelling and control loops can be easily found in [6], [9]–[12].

IV. SUCCESSIVE LOOP CLOSURE IN THE AIRCRAFT

The Successive Loop Closure is defined to be an indirect approach to a multi-rate synthesis of control loop series. Then, the following approximation is often necessary: if the sampling rates for the different control loops are integer multiples of one another, and if the control loops are closed in order according to the sampling rate, the fastest one acts as a unit gain for the slower frequency loops [6], [13].

Following the concept, the faster loops will be placed more internally than altitude and velocity along aircraft axis $\boldsymbol{i_b}$, represented by the angular attitude control (roll, pitch and yaw dynamics). Then, Fig. 2 presents a full blocks diagram representing the 5 control loops implemented:

where the bandwidth factor chosen was 5 times slower for the outer one.

From this figure it is possible to highlight some important notes. The inputs in the Aircraft Model are represented by 4 signals: motor speed (n), aileron (δ_a), elevator (δ_e) and rudder (δ_r) positions. The state variables are 9 signals: altitude (h), velocity along aircraft axis i_b (u), velocity along aircraft axis $-k_b$ (ω), roll (ϕ), pitch (θ), yaw angle (ψ), roll ($\dot{\phi}$), pitch ($\dot{\theta}$), yaw rate ($\dot{\psi}$), sideslip angle (β) and sideslip rate ($\dot{\beta}$).

It is also possible to observe the multi-rate control loops, marked with dashed lines, the slower and faster ones. It means that as the speediest loop runs 5 times against, the slowest one runs only 1 ($t_{ts2} = 0.05sec$).

Concerning the slower loops, the airspeed controller acts directly to the aircraft engine through the motor speed control variable (n). The altitude controller generates its control action on the pitch control loop, in the faster one. As a consequence of the faster loop, the pitch attitude controller computes this action and applies it in the aircraft model through the elevator control surface (δ_e).

Regarding the roll angular attitude, the aircraft model receives its control action from the aileron control surface (δ_a). However, the sideslip control loop (which is set up to keep 0 degrees) performs its responses by the rudder control surface (δ_r). In all loops, saturation blocks were added to respect the constructive aircraft parameters.

V. SIMULATIONS RESULTS

The simulation results are divided into two parts: maneuvers in upward and downward direction. Through these two scenarios, it is possible to show the aircraft stability, regardless the course requested by the pilot.

A. Scenario 1

This first scenario describes a circular path in the upward direction, where it is possible to analyze its maneuverability when harder airspeed control action is necessary.

Figure 3 presents the aircraft angular attitude controlled response performed in this test.

In the beginning, a SetPoint (SP) of linear velocity (V_T) is set up to be $15m/s$, and at 15 seconds the take-off is required. From the positive pitch angles (θ), it can be seen that the aircraft nose is leaning up, reaching a maximum

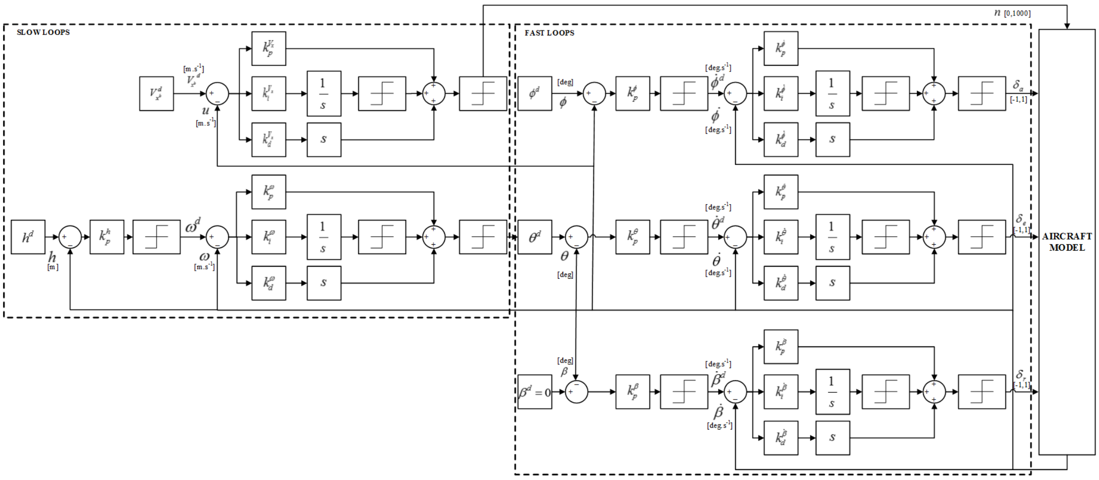

Figure 2. Block diagram of the implemented Successive Loop Closure.

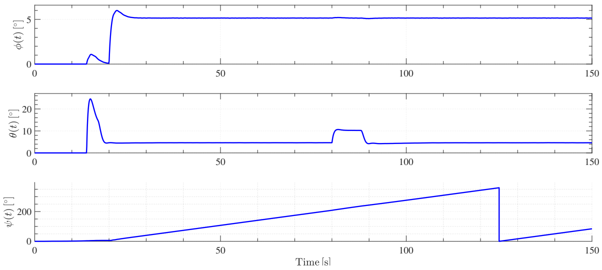

Figure 3. Attitude controlled response of the Simulated Scenario 1.

of 24, 28 degrees. The pitch dynamics stabilizes trimmed at 4, 56 degrees. As a consequence of nose up movements, small disturbances in roll dynamics (ϕ) are noted, quickly corrected.

At 20 seconds, a SP of 5 degrees is requested in roll dynamics (ϕ), presenting an overshoot of 19%. In the instant roll SP, yaw (ψ) maneuvers are noted, due to the sideslip angle (β) control. As observed, the roll SP is kept with the same amplitude until the end of the simulation.

For about 80 seconds, another altitude (h) SP is observed, noting the positive pitch angles again, lasting around 10 seconds.

Following, Fig. 4 presents the aircraft airspeed (V_T), the attack (α) and sideslip (β) angle performed in this scenario.

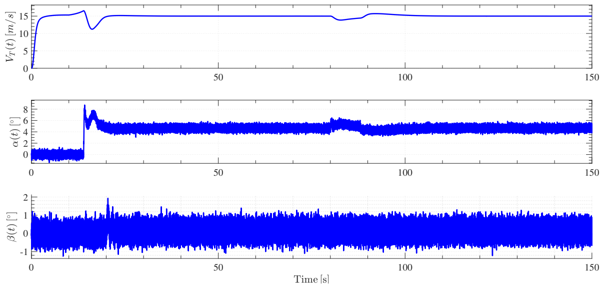

Figure 4. Airspeed, attack and sideslip angles of the Simulated Scenario 1.

From white noise disturbance inserted in the control loops, small variations are perceived in attack and sideslip angles. Concerning to attack angle controlled response (α), it is seen more significant amplitudes when altitude SP is applied (15 seconds of flight) than the rest of simulation, stabilized at 4, 5 degrees. At the instant of another altitude SP, different significant amplitudes are noted in attack angle, lasting around 10 seconds.

Regarding sideslip controlled response (β), it is possible to check that it stays around 0 degrees, as desired. It is important to highlight that this aircraft was projected to keep 0 degrees of sideslip angle, corrected by the rudder control surface, if necessary.

About the motor speed (n), Fig. 5 shows the reference speed from the airspeed control loop and the performed speed executed by the motor. It is noted some variation between them due to its dynamics model taken into account.

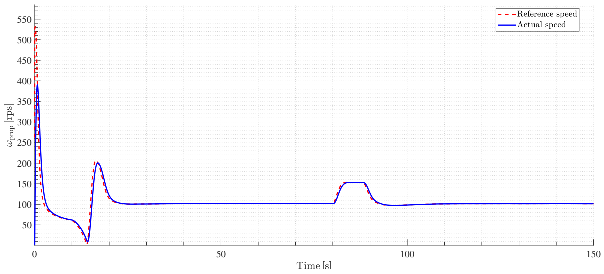

Figure 5. Motor speed performed in Simulated Scenario 1.

At the take-off moment, high reference speeds (n_c) are requested from the airspeed control loop (normal in take-off procedure), tracking it satisfactorily. After that, a decrease in the velocities is observed to avoid altitude overshoot signals. At the instant of the roll (ϕ) SP, an increase in the motor speed is noted to keep the same airspeed SP ($15m/s$), which is stabilized around 101, 6 rps (rotations per seconds). In 80 seconds of simulation, another increase is observed, resulted from the change of altitude SP.

To graphically illustrate the global inertial movements, Fig. 6 is displayed.

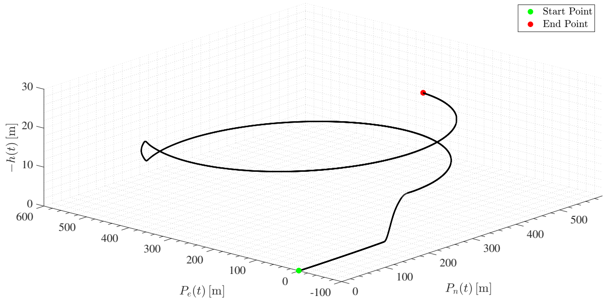

Figure 6. Three-dimensional view performed by the aircraft in Simulated Scenario 1.

B. Scenario 2

This scenario will describe the aircraft maneuverability in downward movements. Therefore, the first ones are the airspeed (V_T) and altitude (h) SPs, $15m/s$ and $30m$, respectively. Before it reaches the $30m$ SP, 20 degrees of roll (ϕ) is set up. To exemplify the angular attitudes, Fig. 7 is displayed.

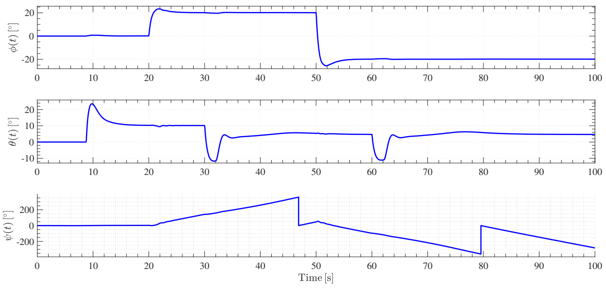

Figure 7. Attitude controlled response of the Simulated Scenario 2.

The take-off is performed at 9 seconds of flight, given a positive pitch angle (θ) responses, obtaining a maximum of $23,51$ degrees. At 20 seconds, the 20 degrees of roll angle (ϕ) are done until 50 seconds. After this instant of time, -20 degrees are desired until the end of the simulation.

Other variants of pitch angles are perceived, explained by the case when altitude SPs change at 30 and 60 seconds. In these situations, the pitch angle is negative due to the aircrafts downward movement.

Concerning yaw dynamics (ψ), it is seen maneuvers in different directions when roll SPs are requested. Another point to highlight is about the yaw speed ($\dot{\psi}$), which is bigger in this scenario than in the first one (Fig. 3). To correct it, the rudder control surface (δ_r) acts eliminating them, turning the aircraft heading as the time passes. To exemplify it, Fig. 8 is displayed.

As it was mentioned, higher sideslip angles are seen in this figure, reaching almost $|10|$ degrees during the simulation. After the presence of sideslip angles, the rudder control surface corrects them, staying stabilized around 0 degrees. The correlation between airspeed and attack angles is observed from their responses. If attack angle has positive increases and exceeds the trimmed value, airspeed SP decreases. The opposite also happens if attack angle has negative increases, which implies the airspeed SP also to increase. After those situations, the controllers corrected these parts.

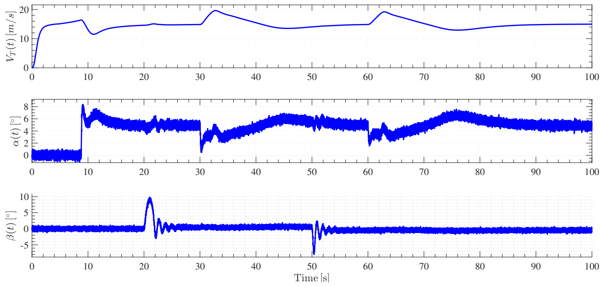

Figure 8. Airspeed, attack and sideslip angles of the Simulated Scenario 2.

The control actions (n_c) sent to be performed by motor speeds (n) are shown in Fig. 9.

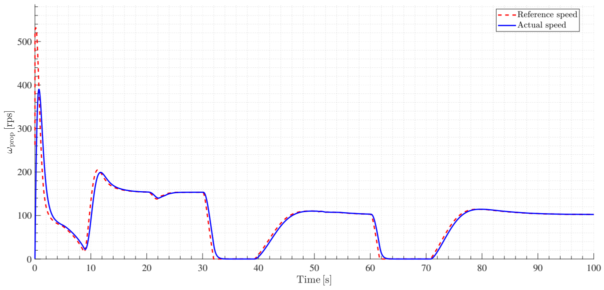

Figure 9. Motor speed performed in Simulated Scenario 2.

Again, at the beginning of the simulation is perceived a firm control action from the airspeed controller, necessary to the take-off part. Around 9 seconds, the altitude SP is required, noting a speed decrease by consequence. For about 20 seconds, small oscillations are seen due to roll SP. At 30 seconds of flight, the altitude SP is changed $-10m$, where the motor speed almost reaches 0 rps, keeping the airspeed in $15m/s$, only through gravitational force. In 60 seconds, this situation is observed again when the altitude SP is also decreased.

For a better understanding of the scenario, Fig. 10 depicts the global inertial positions during the test.

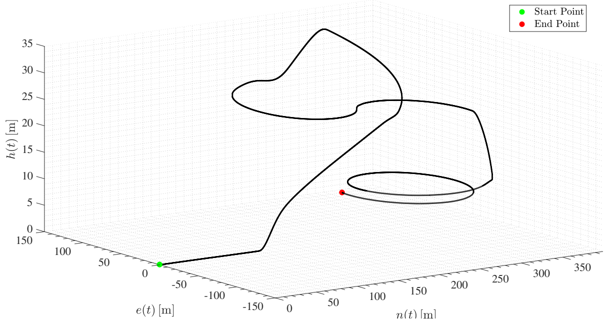

Figure 10. Three-dimensional view performed by the aircraft in Simulated Scenario 2.

VI. CONCLUSIONS

In this paper, techniques of control loop were presented, through P/PID controller in multi-rate loops applied to fixed-wing aircrafts. It was also presented a full kinematics and dynamics model, where the Successive Loop Closure was implemented, connecting and harmonically interacting with them. Another point to highlight is about the tuning of controllers, working in a satisfactory form. From these preliminary simulation tests, it is possible to conclude that this prototype can be tested in experimental field tests. Regarding the Successive Loop Closure technique, nothing unexpected was observed, showing that the interaction between different loop levels was performed well.

These preliminary tests are part of a full project, which means to create a hybrid aircraft, mixing fixed-wing and quadcopter topologies. The next step is the execution of experimental field tests, where after validation process, the introduction of quadcopter topology will be started, as well its modelling and control. Another important stage of this project is the signal estimation, design of over-actuated UAVs, development of new control loop topologies, among others.

As mentioned in Section I, signal estimation (on-line or off-line) and new controller tuning technique through decoupling can be implemented using UAVs. The next step will be lead through the papers [14]–[19]. Another important works about optimization techniques to be followed are [20]–[22].

ACKNOWLEDGMENT

The authors thank INERGE, UFJF, CEFET-MG, CPFL and TBE for the financial support.

REFERENCES

[1] R. Mahony, V. Kumar, and P. Corke, "Multirotor aerial vehicles," *IEEE Robotics and Automation magazine*, vol. 20, no. 32, 2012.

[2] T. Espinoza, A. Dzul, R. Lozano, and P. Parada, "Backstepping-sliding mode controllers applied to a fixed-wing UAV," *Journal of Intelligent & Robotic Systems*, vol. 73, no. 1-4, pp. 67–79, 2014.

[3] J. J. Corona-Sánchez and H. Rodríguez-Cortes, "Lateral-directional control for a fixed wing vehicle based on the total energy control system approach," in *International Conference on Unmanned Aircraft Systems (ICUAS)*, pp. 936–944, IEEE, 2015.

[4] D. J. Grymin and M. Farhood, "Two-step system identification and trajectory tracking control of a small fixed-wing UAV," *Journal of Intelligent & Robotic Systems*, vol. 83, no. 1, pp. 105–131, 2016.

[5] L. Dai and R. N. Jazar, *Nonlinear Approaches in Engineering Applications 2*. Springer, 2012.

[6] R. W. Beard and T. W. McLain, *Small unmanned aircraft: Theory and practice*. Princeton, USA: Princeton University Press, 2012.

[7] F. C. Ferreira, M. F. Santos, and V. B. Schettino, "Computational vision applied to mobile robotics with position control and trajectory planning: Study and application," in *19th International Carpathian Control Conference (ICCC)*, IEEE, 2018.

[8] M. V. Cook, *Flight Dynamics Principles*. New York, USA: Butterworth-Heinemann, 1997.

[9] M. F. Silva, A. C. Ribeiro, M. F. Santos, M. J. Carmo, L. M. Honório, E. J. Oliveira, and V. F. Vidal, "Design of angular PID controllers for quadcopters built with low cost equipment," in *20th International Conference on System Theory, Control and Computing (ICSTCC)*, pp. 216–221, IEEE, Oct 2016.

[10] M. F. Santos, V. S. Pereira, A. C. Ribeiro, M. F. Silva, M. J. Carmo, V. F. Vidal, L. M. Honório, A. S. Cerqueira, and E. J. Oliveira, "Simulation and comparison between a linear and nonlinear technique applied to altitude control in quadcopters," in *18th International Carpathian Control Conference (ICCC)*, pp. 234–239, IEEE, 2017.

[11] V. F. Vidal, L. M. Honório, M. F. Santos, M. F. Silva, A. S. Cerqueira, and E. J. Oliveira, "UAV vision aided positioning system for location and landing," in *18th International Carpathian Control Conference (ICCC)*, pp. 228–233, IEEE, 2017.

[12] M. F. Silva, A. S. Cerqueira, V. F. Vidal, L. M. Honório, M. F. Santos, and E. J. Oliveira, "Landing area recognition by image applied to an autonomous control landing of VTOL aircraft," in *18th International Carpathian Control Conference (ICCC)*, pp. 240–245, IEEE, 2017.

[13] M. C. Berg, "The design of multirate digital control systems," 1986.

[14] E. J. Oliveira, L. M. Honório, A. H. Anzai, L. W. Oliveira, and E. B. Costa, "Optimal transient droop compensator and PID tuning for load frequency control in hydro power systems," *International Journal of Electrical Power & Energy Systems*, vol. 68, pp. 345–355, 2015.

[15] L. M. Honório, A. M. L. da Silva, D. A. Barbosa, and L. F. N. Delboni, "Solving optimal power flow problems using a probabilistic α-constrained evolutionary approach," *IET generation, transmission & distribution*, vol. 4, no. 6, pp. 674–682, 2010.

[16] L. M. Honório, M. Vidigal, and L. E. Souza, "Dynamic polymorphic agents scheduling and execution using artificial immune systems," in *International Conference on Artificial Immune Systems*, pp. 166–175, Springer, 2008.

[17] L. M. Honório, E. B. Costa, E. J. Oliveira, D. de Almeida Fernandes, and A. P. G. Moreira, "Persistently-exciting signal generation for optimal parameter estimation of constrained nonlinear dynamical systems," *ISA transactions*, 2018.

[18] L. M. Honório, D. A. Barbosa, E. J. Oliveira, P. A. N. Garcia, and M. F. Santos, "A multiple kernel classification approach based on a quadratic successive geometric segmentation methodology with a fault diagnosis case," *ISA transactions*, 2018.

[19] M. M. Machado, A. J. Carvalho, M. F. Santos, and J. R. de Carvalho, "Case study: Level and temperature multivariable control and design via arduino through control loop decoupling," in *19th International Carpathian Control Conference (ICCC)*, IEEE, 2018.

[20] L. C. Gonçalves, M. F. Santos, R. J. F. de Sá, J. L. da Silva, H. B. Rezende, *et al.*, "Development of a PI controller through an ant colony optimization algorithm applied to a SMAR® didactic level plant," in *19th International Carpathian Control Conference (ICCC)*, IEEE, 2018.

[21] F. F. Panoeiro, M. F. Santos, D. C. Silva, J. L. Silva, and M. J. Carmo, "PI controller tuned by bee swarm for level control systems," in *19th International Carpathian Control Conference (ICCC)*, IEEE, 2018.

[22] J. M. S. Ribeiro, M. F. Santos, M. J. Carmo, and M. F. Silva, "Comparison of PID controller tuning methods: analytical/classical techniques versus optimization algorithms," in *18th International Carpathian Control Conference (ICCC)*, pp. 533–538, IEEE, 2017.

APPENDIX A

As mentioned in Section II-B, Γ_* equations are expressed below.

$$\begin{aligned}
\Gamma_1 &= \frac{J_{xz}(J_x - J_y + J_z)}{\Gamma}, & \Gamma_2 &= \frac{J_z(J_z - J_y) + J_{xz}^2}{\Gamma}, \\
\Gamma_3 &= \frac{J_z}{\Gamma}, & \Gamma_4 &= \frac{J_{xz}}{\Gamma}, \\
\Gamma_5 &= \frac{J_z - J_x}{J_y}, & \Gamma_6 &= \frac{J_{xz}}{J_y}, \\
\Gamma_7 &= \frac{(J_x - J_y)J_x + J_{xz}^2}{\Gamma}, & \Gamma_8 &= \frac{J_x}{\Gamma}, \\
\Gamma_9 &= J_x J_z - J_{xz}^2.
\end{aligned}$$

where $\Gamma = J_x J_z - J_{xz}^2$, J_x means inertia moment taking $\boldsymbol{i^b}$ axis in account, J_y means inertia moment in $\boldsymbol{j^b}$ axis, J_z means inertia moment in $\boldsymbol{k^b}$ axis, J_{xz} the product of inertia around $\boldsymbol{i^b} - \boldsymbol{k^b}$ plane.